Economic assessment of membrane-assisted autothermal reforming for cost effective hydrogen production with CO_2 capture

*Schalk Cloete[1], Mohammed N. Khan[2], Shahriar Amini[1]**

[1] SINTEF Industry, Trondheim, Norway

[2] Norwegian University of Science and Technology, Trondheim, Norway

*Corresponding author:

Shahriar Amini

S.P. Andersens vei 15B, 7031 Trondheim, Norway

+4746639721

shahriar.amini@sintef.no

Abstract

A recent techno-economic study (Spallina *et al.*, Energy Conversion and Management 120: p. 257-273) showed that the membrane assisted chemical looping reforming (MA-CLR) technology can produce H_2 with integrated CO_2 capture at costs below that of conventional steam methane reforming. A key technical challenge related to MA-CLR is the achievement of reliable solids circulation between the air and fuel reactors at large scale under the high (>50 bar) operating pressures required for optimal performance. This work therefore presents process modelling and economic assessments of a simplified alternative; membrane assisted autothermal reforming (MA-ATR), that inherently avoids this technical challenge. The novelty of MA-ATR lies in replacing the MA-CLR air reactor with an air separation unit (ASU), thus avoiding the need for oxygen carrier circulation. The economic assessment found that H_2 production from MA-ATR is only 1.5% more expensive than MA-CLR in the base case. The calculated cost of hydrogen (compressed to 150 bar) in the base case was 1.55 €/kg with a natural gas price of €6/GJ and an electricity price of €60/MWh. Both concepts show continued performance improvements with an increase in reactor pressure and temperature, while an optimum cost is achieved at about 2 bar H_2 permeate pressure. Sensitivities to other variables such as financing costs, membrane costs, fuel and electricity prices are similar between MA-ATR and MA-CLR. Natural gas prices represent the most important sensitivity, while the sensitivity to membrane costs is relatively small at high reactor pressures. MA-ATR therefore appears to be a promising alternative to achieve competitive H_2 production with CO_2 capture if technical challenges significantly delay scale-up and deployment of MA-CLR technology. The key technical demonstration required before further MA-ATR scale-up is membrane longevity under the high reactor pressures and temperatures required to minimize the cost of hydrogen.

Keywords: H_2 production, Chemical looping reforming, Membranes, Autothermal reforming, CO_2 capture.

1 Introduction

Given the consensus about anthropogenic climate change [1] and the Paris Climate Accord ambition of limiting global temperature rise well below 2 °C [2], hydrogen is receiving increased attention as an energy carrier for a future carbon-constrained world. An important challenge facing the hydrogen economy is that the vast majority of current production comes from fossil fuels with large associated CO_2 emissions, mainly steam-methane reforming (SMR) [3].

Clean hydrogen production from renewable energy via electrolysis is gaining increased attention, but these methods remain expensive relative to thermochemical conversion of fossil fuels [4, 5]. Another method for producing carbon-free hydrogen is the addition of CO_2 capture and storage (CCS) to conventional processes, but this increases the hydrogen cost by 40-100% [6].

One promising method for reducing the cost of hydrogen production with CO_2 capture is chemical looping reforming (CLR) [7, 8]. The CLR concept is based on the principle of chemical looping combustion (CLC) [9, 10], where an oxygen carrier material extracts oxygen from air and delivers it to a fuel to allow hydrocarbon combustion without any mixing of N_2 and CO_2. Whereas the production of high grade heat for power production is the primary objective of CLC, CLR utilizes the CLC principle to achieve autothermal reforming without the need for an air separation unit (ASU) or dilution of the produced syngas with N_2.

The attractiveness of CLR can be further enhanced by inserting membranes into the fuel reactor [11]. Membranes extract hydrogen directly from the reformer, avoiding the need for downstream water-gas shift and pressure swing adsorption units. It also shifts the equilibrium of the reforming reactions to produce more H_2, thus allowing for operation at much lower temperatures with the same degree of fuel conversion. Economic performance of this membrane-assisted chemical looping reforming (MA-CLR) concept has recently been evaluated by Spallina, Pandolfo [12] to find that hydrogen can be produced significantly below the cost of conventional SMR. The potential of producing clean hydrogen at a lower cost than conventional carbon-intensive methods is highly attractive and deserves substantial further research attention.

Spallina, Pandolfo [12] also evaluated another fluidized bed membrane reactor technology originally proposed by Gallucci, Van Sint Annaland [13]. This reactor uses a single fluidized bed – a significant simplification relative to MA-CLR – but requires additional H_2 perm-selective membranes fed with air to supply the heat for reforming by combusting permeated H_2. In addition, a cryogenic CO_2 purification unit is required to separate CO_2 exiting the reactor from the H_2 and CO that slipped past the membranes. The techno-economic assessment showed that H_2 production from this concept was 15% more expensive than MA-CLR, while CO_2 avoidance was 19 %-points lower [12].

Such fluidized bed membrane reactors are a more recent research interest. Originally, most membrane reactor concepts were proposed as packed beds [14] or catalyst-coated channels [15]. However, static configurations suffer from significant temperature and concentration polarization, which can cause these reactors to require double the membrane surface area of an equivalent fluidized bed reactor where these limitations are avoided by excellent mixing [16]. For this reason, a thorough review by Gallucci, Fernandez [17] concluded that fluidized beds are the better choice for H_2 production from methane reforming. These reactors have been demonstrated experimentally [18-22].

MA-CLR appears to be the most promising membrane fluidized bed reactor concept from an economic point of view [12], but it faces an important technical challenge: achieving steady oxygen carrier circulation under the high pressures required to minimize membrane surface area and maximize process efficiency. The oxygen carrier material needs to be transported through cyclones, loop seals and solids transport lines between the air and fuel reactors. Good performance of the MA-CLR concept is completely dependent on reliable circulation of the oxygen carrier to supply heat to the reforming reactions and to convert the remaining fuel gases slipping past the membranes.

After two decades of active R&D, the vast majority of chemical looping experimental studies have been performed at atmospheric pressure with only a few studies at moderate pressures up to 5 bar [23, 24]. It will therefore be a long time before chemical looping technology is available at the scale (fuel reactor 2.9 m in diameter and 13 m in height) and pressure (50 bar) used in the aforementioned highly attractive economic assessment [12].

Due to this technical challenge, the present work considers a simplified membrane assisted autothermal reforming (MA-ATR) concept where a single reactor without solids circulation is used. The reactor concept is similar to the fluidized bed membrane reactor successfully operated under autothermal reforming mode by Mahecha-Botero, Boyd [25] and modelled by Mahecha-Botero, Grace [26]. The MA-ATR concept evaluated in this work differs from the aforementioned works [25, 26] in the use of high-purity O_2 as the oxidant and the use of a catalyst that also performs as an oxygen carrier to maximize fuel and O_2 conversion to allow stoichiometric O_2 addition.

As illustrated in Figure 1, the reactor is essentially identical to the fuel reactor in the MA-CLR process. Methane and steam are injected at the bottom of the reactor and are reformed to syngas over the fluidized Ni-based oxygen carrier that also acts as a catalyst. The membranes continuously extract H_2 from this reforming region of the reactor, shifting the equilibrium of the reactions towards greater fuel conversion. Some unconverted fuel slips past the membranes to react with oxidized Ni-based oxygen carrier (NiO) above the membranes. The way in which NiO is generated is where MA-ATR differs from MA-CLR: instead of receiving hot oxidized oxygen carrier from the air reactor, the oxygen carrier is oxidized above the membranes with high purity O_2 from an air separation unit (ASU). The role of the oxygen carrier is therefore not to transfer oxygen from the air reactor to the fuel reactor, but rather to ensure complete conversion of the fuel that slips past the membranes and to transport the generated heat to the lower regions of the reactor where the endothermic SMR reactions take place.

As this work will show, the use of an ASU brings only small increases to the cost of hydrogen. Compression of air to the high reactor operating pressures in MA-CLR requires significant electricity consumption that is avoided by MA-ATR. In addition, the N_2 in the air fed to the MA-CLR air reactor requires significant fuel combustion to heat it up to the reactor temperature, reducing the hydrogen yield. From a capital cost point of view, some of the added cost of including the ASU is cancelled out by the lower reactor cost and avoidance of the turbomachinery required to compress the air and recover energy from the air reactor outlet.

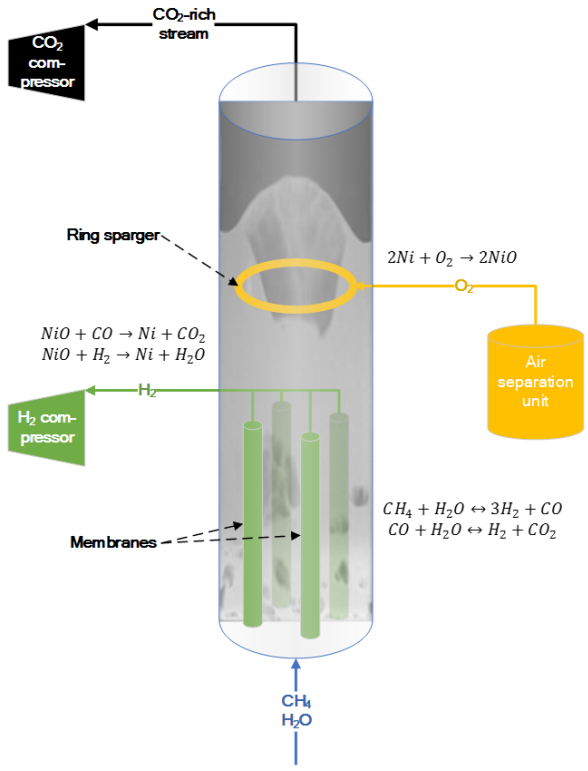

Figure 1: Illustration of the MA-ATR concept assessed in this work. The reactions indicate that reforming takes place in the lower regions around the membranes, oxygen carrier reduction with slipped fuel takes place directly above the membranes, and oxygen carrier oxidation with evenly injected oxygen from the ASU takes place in the upper regions.

Another important benefit of MA-ATR over MA-CLR is that the gentle bubbling fluidized bed reactor in MA-ATR will have much lower particle attrition and elutriation than the circulating fluidized bed setup

in MA-CLR. This will allow for the use of a well-established Ni-based oxygen carrier and catalyst that has relatively high costs and significant human health impacts [27]. Despite continued efforts to develop alternatives, Ni-based CLR oxygen carriers remain superior in terms of reactivity, selectivity and mechanical stability. Given that the MA-ATR reactor will minimize elutriation of Ni-containing fines and can easily filter out these fines from the single outlet stream (after cooling), the cost and health impacts of Ni-based oxygen carriers will be minimized.

From an operational point of view, the MA-ATR concept will also make it simpler to ensure a uniform distribution of NiO above the membranes to avoid fuel slip from the reactor. O_2 from the ASU can be injected uniformly via a ring sparger to produce NiO uniformly over the reactor cross-sectional area. Such a uniform distribution will be harder to achieve with the concentrated stream of oxidized oxygen carrier entering from the top of the fuel reactor in MA-CLR, especially if the reactor diameter is large.

Overall, the MA-ATR concept can avoid the technical challenges related to the circulation of large quantities of oxygen carrier between reactors operating at very high pressures for a modest increase in cost relative to MA-CLR. The MA-ATR concept should therefore still be able to compete with current commercial hydrogen production processes without any price on CO_2 even while capturing 100% of the produced CO_2.

The remainder of this work will detail a comparative thermodynamic and economic assessment between MA-CLR and MA-ATR. Comparisons will be carried out over a range of pressures inside and outside the membranes as well as other important variables like fuel and electricity prices.

2 Methodology

The cases studied in this work covered three pressure levels in the reactor (25, 50 and 100 bar), three pressure levels inside the membranes (1, 2, and 4 bar), as well as three reactor temperature levels (600, 700 and 800 °C) for both the MA-ATR and MA-CLR processes. Increasing the reactor pressure will reduce the required membrane surface area due to a higher driving force for hydrogen permeation into the membrane. Increasing the pressure inside the membrane (H_2 permeate pressure) will require a larger membrane surface area, but create savings in the energy and capital costs related to hydrogen compression. Increasing the reactor temperature will reduce the required membrane surface area by increasing the H_2 concentration in the reactor because the steam-methane reforming reaction is thermodynamically favoured at higher temperatures.

2.1 Plant description and process modelling

2.1.1 Membrane assisted chemical looping reforming (MA-CLR)

The MA-CLR plant configuration used in this study is similar to that described by Spallina, Pandolfo [12]. The process flow diagram of the plant is shown in Figure 2 and stream data for the base case can be found in the appendix (Table 11). Firstly, the natural gas is pre-heated to 324 °C to convert any sulfur compounds to hydrogen sulfide (H_2S). The pre-heated gas is then passed over a bed of zinc oxide (ZnO) in the desulfurizer where H_2S is adsorbed. This process is not modeled in detail as it is insignificant to the outcome of the current study. Downstream of the desulfurizer, the natural gas is mixed with steam, maintaining a steam-to-carbon ratio of 1.75. This mixture is reformed to remove higher hydrocarbons at 490 °C using a nickel-based catalyst in a pre-reformer, thus minimizing the coke

deposition in the process. The pre-reformed natural gas is further heated to 454 ℃ before introducing it into the chemical looping reforming (CLR) unit.

The CLR unit consists of a fuel reactor (FR) and an air reactor (AR). As opposed to conventional CLR system, this configuration has palladium (Pd) membranes inserted into the bed material to extract H_2. Nickel oxide (NiO) is considered as the oxygen carrier and is supported on $NiAl_2O_4$ for mechanical stability. The natural gas enters the FR and reacts with NiO to form CO_2 and H_2O. Furthermore, the reduced nickel (Ni) acts as a catalyst for the steam-methane reforming (SMR) and water-gas shift (WGS) reactions. The retentate stream consisting of CO_2 and H_2O is captured from the top of the FR while the H_2 produced during the process permeates through the membranes. The reduced OC is supplied to the AR where it is partially oxidized and fed into the FR from the top. This ensures that the unreacted fuel that may have slipped reacts with fresh OC above the membranes to convert it to CO_2 and H_2O while reducing NiO to Ni.

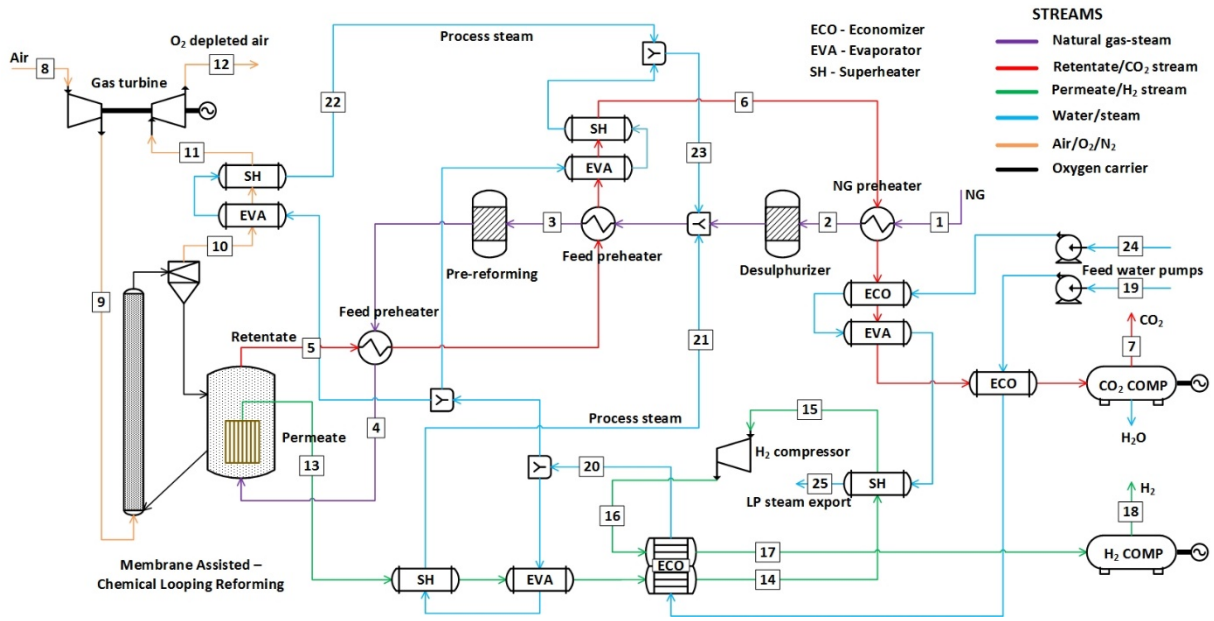

Figure 2: Schematic of membrane assisted chemical looping reforming plant.

The retentate is used to pre-heat the natural gas and to produce superheated process steam and saturated low pressure (LP) steam for export. After H_2O condensation, the CO_2 is compressed and sent for storage. The permeated H_2 is used to produce part of the process steam and superheat the LP steam before being compressed and recirculated for pre-heating the process feed water. Finally, the H_2 is compressed to 150 bar for ease of storage and transportation. The high-temperature O_2 depleted stream from the AR is used to produce the rest of the process steam and then expanded before releasing into the atmosphere.

As mentioned earlier, the CLR reactors are operated at very high pressures up to 100 bar. Therefore, an intercooled air compression is employed to restrict the temperature at the compressor outlet to around 500 °C. This is to avoid damage to the compressor material due to high temperature and pressure conditions. A two-stage and a three-stage compression system is used for the 50 bar and 100 bar cases, respectively. The process steam is superheated to 275 °C for the reactor pressures 25 and 50 bar whereas it is superheated to 321 °C for the reactor pressure of 100 bar. The LP steam for export is generated at 6 bar and 170 ℃.

In addition, the base case is operated at different reforming temperatures (600 – 800 °C) to assess the influence of temperature on the overall performance. The corresponding oxidation temperature is set 200 °C higher than the reforming temperature, i.e. 800 – 1000 °C. For the case at 600 °C, the retentate is used only for preheating the natural gas and the water. About 15% of the superheated process steam is produced using the air reactor exhaust stream while the rest of the steam is produced using the permeate H_2 stream. Unlike other cases, the permeate stream is compressed and recirculated into the evaporator, similar to the configuration for MA-ATR described in Figure 3. For the case at 800 °C, about 45% of the superheated process steam is produced by cooling the air reactor exhaust stream. The rest of the steam is produced using the permeate stream without any compression and recirculation requirement. It is further cooled to produce part of the low-pressure saturated steam. On the other hand, the retentate is used to preheat the natural gas, water for the process and water for the LP steam.

2.1.2 Membrane assisted autothermal reforming (MA-ATR)

The proposed MA-ATR plant is shown in Figure 3 and stream data for the base case can be found in the appendix (

). In this configuration, a fluidized bed reactor consisting of Pd membranes that are inserted into the bed material is considered. It is similar to the FR of the MA-CLR system while an air separation unit (ASU) replaces the AR as mentioned earlier.

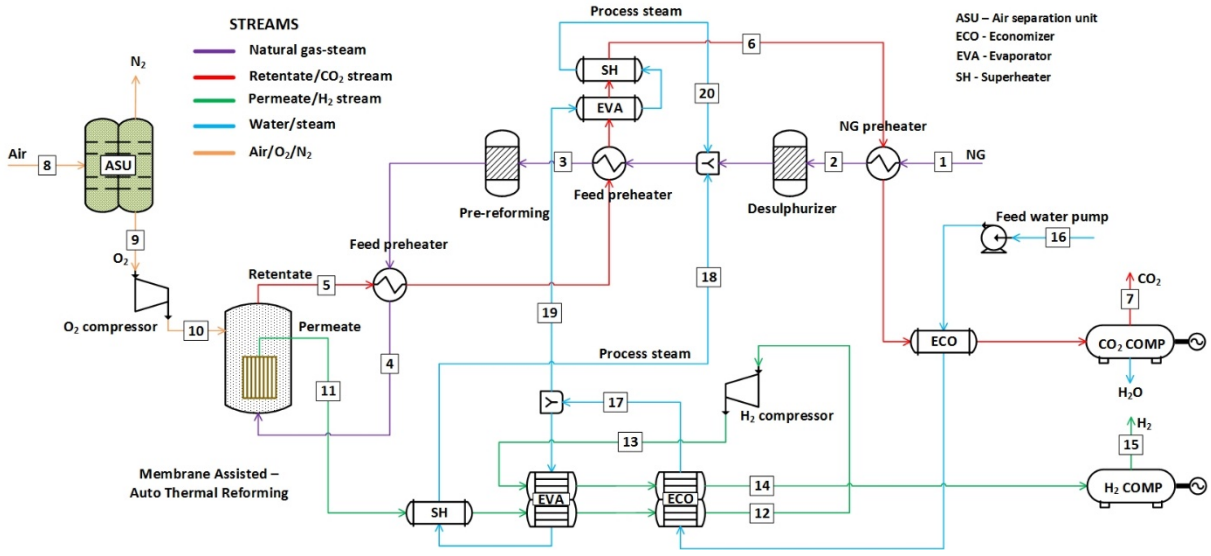

Figure 3: Schematic of membrane assisted autothermal reforming plant.

The ASU is simulated as a double column cryogenic distillation process as shown in Figure 4. The air is compressed in four compression stages to 1.7, 2.6, 3.9 and 5.2 bar, respectively. The compressed air then enters a temperature swing adsorption (TSA) unit where water and CO_2 are removed. The compressed air is split into two streams, cooled in the main heat exchanger (MHE) by the product streams to -175 °C and throttled before being distilled in a high pressure distillation column (5.1 bar). The products are pure nitrogen (N_2) at the top and O_2 enriched air (about 36% vol.) at the bottom. Both these streams are cooled further in an additional heat exchanger (HE) by the N_2 product stream followed by throttling and subjected to low pressure distillation at 1.1 bar. The condenser in the HP column is thermally integrated with the reboiler of the LP column. Here, the products are 95% pure O_2

at the bottom (4.7 bar) and 99.5% pure N_2 at the top (1.1 bar). These product streams are heated in the MHE to 13 ℃. More details can be found in Fu and Gundersen [28].

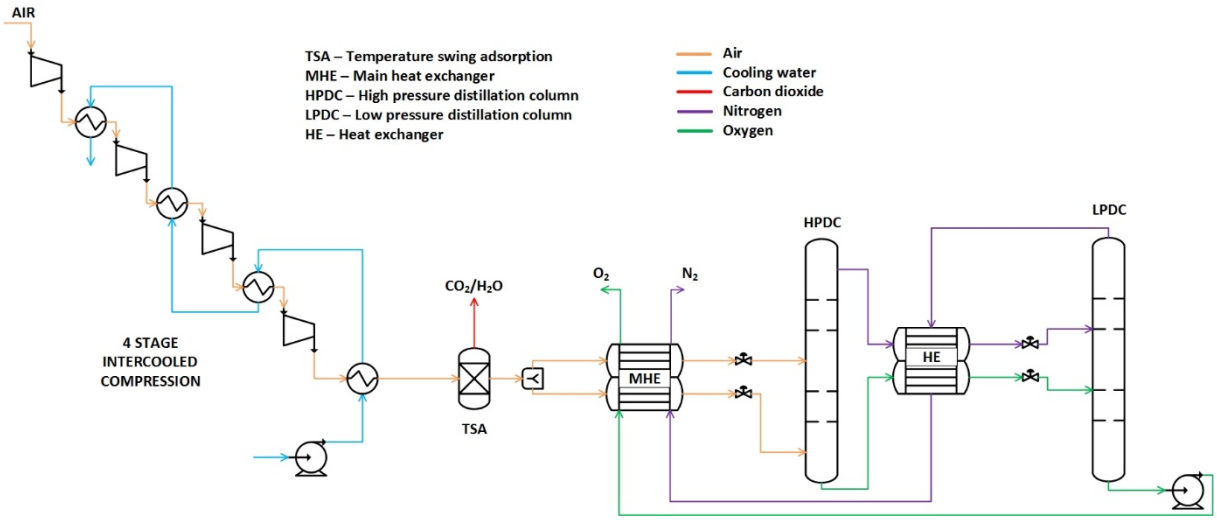

Figure 4: Schematic of a double-column cryogenic air separation unit.

The O_2-rich stream from the ASU is compressed to the required pressures and fed into the reactor to oxidize Ni to NiO. The N_2 is released into the atmosphere but could be compressed and delivered for useful purposes. After the desulfurization step, the pre-reforming is carried out at 440 °C. The resulting CH_4-rich stream is then fed to the MA-ATR reactor to be reformed to syngas, while the pure H_2 permeates through the membranes. Fuel gases slipping past the membranes react with NiO to form CO_2 and H_2O, which exit at the top of the reactor.

Similar to the MA-CLR system, the retentate is used to pre-heat the natural gas, produce some superheated process steam, and pre-heat the feed water before being compressed and sent for storage. The permeate is used to produce the rest of the process steam. In this configuration, due to the absence of a high-temperature heat source (O_2 depleted stream from the AR in case of MA-CLR), no LP steam is produced for export. The permeate is compressed to higher pressures and recirculated into the boiler to produce the required process steam before being compressed for storage.

For the base case, the effect of reforming temperature on the overall performance is also investigated. The temperature is varied from 600 – 800 °C. For the case at 600 °C, the retentate is enough to preheat the natural gas and the water for process steam. About 78% of the superheated process steam is produced by cooling the permeate stream while the rest of the steam is produced by cooling the natural gas and steam fed to the MA-ATR reactor to 319 °C. This lower reactor inlet temperature would reduce the H_2 yield slightly but was required to produce the required steam to maintain the S/C ratio of 1.75. For the case at 800 °C, the configuration is not changed from Figure 3. However, it required less compression of the permeate stream before recirculation into the evaporator, thus saving some compressor power.

2.1.3 Process modeling methodology and assumptions

The mass and energy balances for both the plants are solved using Aspen Plus V10. Thermodynamic equilibrium is assumed and the property method adopted is Redlich-Kwong-Soave equation-of-state with the Boston-Mathias alpha function (RKS-BM). The desulfurizer and pre-reforming are modeled using RGIBBS reactor model, which assumes chemical and phase equilibrium based on the Gibbs

energy minimization concept. The stream information from the 0D model described in the next section is used as input to the plant simulations. In the case of MA-ATR, 95% pure O_2 is produced in ASU and the other assumptions considered are similar to that of Fu and Gundersen [28]. The main assumptions adopted for the plant simulations are listed in Table 1.

Table 1: Main assumptions for plant modelling

	MA-CLR	MA-ATR
Pre-reforming temperature, °C	490	440
Steam-to-carbon ratio	1.75	1.75
Reactor pressure drop, % of inlet pressure	1%	1%
Reforming pressure, bar	25-100	25-100
Permeate pressure, bar	1-4	1-4
Reforming temperature, °C	600-800	600-800
Air/O_2 compressor isentropic efficiency	92.5%	85%
Gas expander isentropic efficiency	92.5%	-
Mechanical efficiency	98%	98%
Steam export pressure, bar	6	-
O_2 purity	-	95%
Heat exchangers		
ΔT_{min} gas-gas/gas-liquid, °C	10/8	
Pressure drop, % of inlet pressure	1%	
H_2 compression		
Compression stages	3	
Final H_2 conditions, °C /bar	30/150	
CO_2 compression		
Compression stages	Depending on the retentate pressure	
Final CO_2 conditions, °C /bar	30/110	
Compressors isentropic efficiency	85%	
Natural gas		
Mol fractions (CH_4, C_2H_6, C_3H_8, C_4H_{10}, CO_2, N_2)	0.89, 0.07, 0.01, 0.0011, 0.02, 0.0089	
Temperature	15 °C	
Pressure	70 bar	

2.2 Reactor modelling

Two types of reactor modelling were employed in this study. A simple 0D mass and energy balance model was used to describe the reactor behaviour for coupling to the process simulations. Key assumptions in this model are outlined in Table 2 and were selected for maximum similarity to the MA-CLR case evaluated by Spallina, Pandolfo [12].

From these model inputs, mass and energy balances were solved to yield the required air or O_2-rich stream inlet flowrates (to supply the oxygen for fuel combustion to achieve autothermal operation), the outlet flowrate of 100% pure H_2 from the membranes, and the outlet compositions of the CO_2 rich stream from the MA-ATR or MA-CLR fuel reactor and the N_2-rich stream from the MA-CLR air reactor (assuming complete fuel and O_2 conversion). Temperature-dependent enthalpy data for individual gas species was taken from the JANAF tables [29].

Table 2: Inputs to the 0D model used in the plant simulations.

Both concepts	
Fuel inlet flowrate	7.56 kg/s
Fuel inlet temperature	454 °C
Fuel inlet mol fractions (H_2, CH_4, H_2O, CO_2, N_2)	0.056, 0.334, 0.580, 0.027, 0.003
Outlet temperature of CO_2 and H_2 streams	700 °C
Steam to carbon ratio	1.75
Fuel and O_2 conversion	100%
MA-ATR	
O_2 -rich stream mol fractions (O_2, N_2)	0.95, 0.05
O_2 stream temperature at 25, 50 and 100 bar	216, 326 and 454 °C
MA-CLR	
Air inlet mol fractions (H_2O, O_2, N_2, Ar)	0.009, 0.208, 0.774, 0.009
Air inlet temperature at 25, 50 and 100 bar	466, 500 and 501 °C
Outlet temperature from air reactor	900 °C

Subsequently, reactor sizing for the economic assessment was completed using a 1D reactor model identical to the one utilized in Wassie, Cloete [30] to assess a more complex membrane assisted gas switching reforming concept. The model was developed in ANSYS FLUENT. In the present work, the model was applied to the MA-ATR reactor and the MA-CLR fuel reactor. The model includes reaction rate expressions for the reforming [31, 32] and oxygen carrier redox [33] reactions, the membrane permeation law given in Equation 1 [34], modelling of axial dispersion of solids species and heat [35], and modelling to account for the momentum [36] and mass [37] transfer limitations imposed by the formation of bubbles in the fluidized bed. No attempt was made to model concentration polarization outside the membranes due to the excellent mixing characteristics of fluidized bed reactors [16]. The interested reader is referred to the appendix of the aforementioned study [30] for more details.

$$F_{H_2} = \frac{P_0}{t_m} e^{\left(\frac{-E_A}{RT}\right)} \left(P_{H_2,ret}^{0.74} - P_{H_2,perm}^{0.74}\right) \frac{\text{mol}}{\text{m}^2\text{s}} \quad \text{Equation 1}$$

Where $P_0 = 4.24 \times 10^{-10} \frac{\text{mol}}{\text{s m Pa}^{0.74}}$, $E_A = 5810 \frac{\text{J}}{\text{mol}}$ and $t_m = 5 \times 10^{-6}$ m.

To standardize the reactor simulations between the different cases studied in this work, common assumptions were applied to all simulation cases as detailed in Table 3. For the MA-CLR case, the oxygen carrier was injected with the same temperature (900 °C) as in Spallina, Pandolfo [12]. However, while Spallina, Pandolfo [12] used an isothermal reactor model, the present study assumes more realistic reactor behaviour where the temperature reduces towards the bottom of the reactor because of imperfect mixing in the fluidized bed. An earlier study [38] showed that accounting for this effect can increase the required membrane surface area by about 10% relative to the ideal isothermal case.

Non-isothermal reactor modelling caused the temperature at the bottom of the reactor, where the oxygen carrier is extracted, to be lower than the 700 °C assumed by Spallina, Pandolfo [12]. To ensure that cooling of the oxygen carrier will supply the same amount of heat to the reactor in each case, the oxygen carrier injection rate was varied inversely proportionally to the temperature difference between the injection and extraction points from the reference injection rate of 132.66 kg/s for a 200

°C temperature drop [12]. This simple relation could be implemented because of the assumption of a constant oxygen carrier heat capacity (Table 3). Similarly, the active content of the oxygen carrier was varied inversely proportionally to the calculated mass flow rate to ensure that the same flowrate of active material is injected in each case. In this way, the inflow of NiO was kept constant at 11.65 kg/s for all cases to be consistent with Spallina, Pandolfo [12].

Table 3: Assumptions in the 1D reactor modelling.

Reactor aspect ratio	3
Membrane height	Lower 60% of the reactor
Membrane volume fraction	0.5
Membrane diameter	0.05 m
Minimum P_{H_2} difference over membrane	0.2 bar
Oxygen carrier density	3400 kg/m^3
Oxygen carrier particle size	150 µm
Oxygen carrier heat capacity	1200 J/kg.K
Oxygen injection in MA-ATR	At 70% of the reactor height
Oxygen carrier insertion in MA-CLR	At 80% of the reactor height
Oxygen carrier extraction in MA-CLR	At bottom of the reactor

Given the very high reactivity of the Ni-based oxygen carrier and catalyst employed in the simulations, the membranes are the rate-limiting step. The reactor size can therefore be minimized by maximizing the area density of membranes in the reactor. A dense packing of membranes, occupying a volume fraction of 0.5 in the lower 60% of the reactor, was therefore implemented to minimize reactor costs. The membrane diameter and minimum H_2 partial pressure difference over the membrane were selected to be identical to Spallina, Pandolfo [12].

For MA-CLR, the oxidized oxygen carrier from the air reactor was assumed to fall on top of the bed expanding up to 80% of the reactor height. Fully reduced oxygen carrier is assumed to exit from the bottom of the simulated fuel reactor to be transported back to the air reactor to be re-oxidized. In MA-ATR, the O_2 was injected below the expanded bed surface at 70% of the reactor height to give the injected oxygen sufficient residence time to react with the oxygen carrier material. These assumptions were found to achieve full conversion of slipped fuel and injected oxygen in the reactor simulations.

Using these assumptions, the reactor height was varied iteratively in each simulated case until the point just before fuel slip out of the reactor starts to take place. This is the point where the optimal reactor performance assumed in the 0D models is achieved with the smallest reactor size and membrane surface area. As an illustration, axial profiles from the base case are shown in Figure 5.

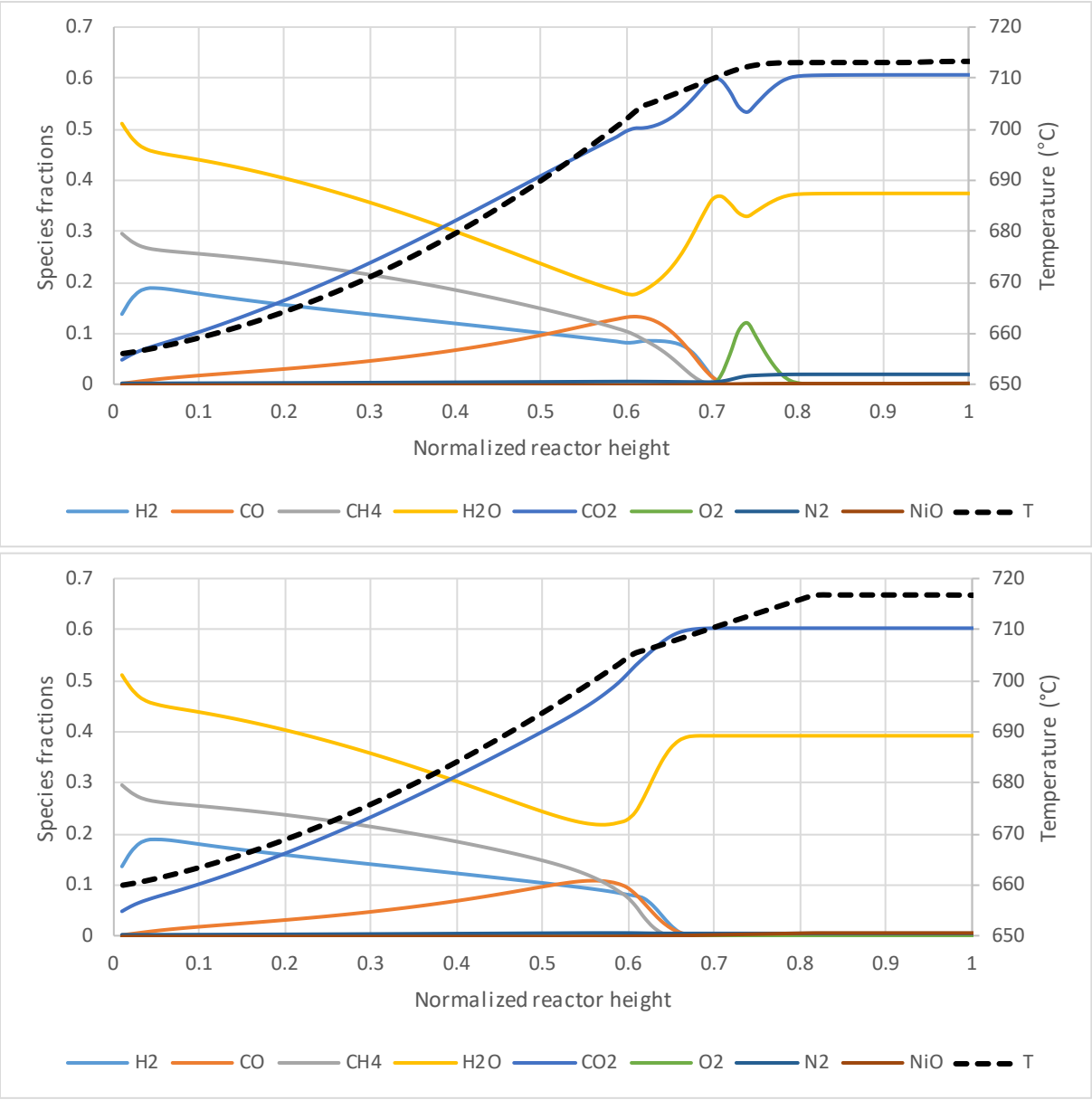

Figure 5: Axial profiles of gas species mol fractions, NiO mass fraction and reactor temperature for the MA-ATR (top) and MA-CLR (bottom) cases. The reactor pressure was set to 50 bar and the hydrogen permeate pressure to 1 bar.

The reactor behaviour in the membrane zone (bottom 60% of the reactor) is very similar between the MA-ATR and MA-CLR cases. As the gas rises through the reactor, the CH_4, H_2 and H_2O fractions drop as H_2 is continuously extracted by the membranes, while the fractions of CO and CO_2 increase. Once the gases pass the membranes, the behaviour changes as fuel gases get in contact with NiO to be converted to H_2O and CO_2. In the MA-ATR concept, the NiO is generated by an O_2-rich stream from the ASU injected at 70% of the reactor height (the O_2 spike is clearly visible in Figure 5, top), while the NiO is directly injected into the reactor at 80% of the reactor height in the MA-CLR case. Due to the rapid axial diffusion of NiO through the bed, the mass fraction of NiO is barely visible in Figure 5.

As indicated by the temperature profiles, however, the mixing in the fluidized bed is not perfect. A temperature drop of more than 50 °C is observed from the top of the bed (where the exothermic oxidation happens in MA-ATR and the hot oxygen carrier is injected in MA-CLR) to the bottom of the reactor. Figure 5 shows that this temperature drop is a little faster for MA-ATR than MA-CLR. This is

because MA-CLR must complete a little more combustion and a little less reforming than MA-ATR to also heat up the air in the air reactor. A lower amount of endothermic reforming results in a smaller temperature drop through the reactor.

The lower level of reforming required in MA-CLR means that slightly higher H_2 concentrations can be afforded at the top of the membrane region where fuel starts to be combusted instead of being reformed. This small increase in H_2 fraction in MA-CLR relative to MA-ATR is barely discernible in Figure 5, but generally allows the MA-CLR reactor to be slightly smaller than the MA-ATR reactor because of a slightly larger driving force for H_2 extraction.

2.3 Economic assessment

2.3.1 Capital costs

Three different methods were followed to determine the capital costs of the plant. For common equipment including heat exchangers, pumps, compressors and turbines, the module costing method of Turton, Bailie [39] was followed. This broadly accepted method for chemical plant cost estimation utilizes cost functions for equipment purchase costs under reference conditions (generally atmospheric pressure equipment constructed from carbon steel) and several multipliers accounting for installation costs, higher operating pressures and more expensive construction materials. The resulting installed cost of each component is referred to as the bare module cost.

All bare module costs determined via be module costing method were adjusted for inflation to the year 2016 by a CEPCI factor of 542/397 and from US dollars to Euros using an exchange rate of 1.2 $/€.

Given the high operating pressures required in the MA-ATR and MA-CLR plants, the pressure multiplier was an important factor in the analysis. In addition, more expensive stainless steel construction material was selected for all components dealing with fuel gases or CO_2. Standard carbon steel was selected for components only exposed to air.

Reactor costs were also estimated using the method of Turton, Bailie [39] by assuming that the reactor is composed of two process vessels: a thick outer pressure shell constructed from carbon steel to withstand the reactor operating pressure and a Ni-alloy inner reactor vessel at atmospheric pressure separated by a 20 cm layer of vermiculite insulation material. The outer vessel carries the pressure load, while the inner vessel carries the thermal, corrosion and attrition loads. The 20 cm insulation is sufficient to ensure negligible heat losses. The cost of the inner Ni-alloy vessel was doubled to account for the cost of reactor elements like a gas distributor plate and O_2 injection sparger.

Initial oxygen carrier loading was added to the reactor capital cost, assuming that 25% of the reactor volume is filled with oxygen carrier costing $15/kg [27]. For MA-CLR, the total reactor cost is doubled from the MA-ATR cost estimate because MA-CLR requires an extra air reactor, cyclone, loop seals and solids transport lines. This is a crude assumption, but, as will be illustrated in a later sensitivity study, only has a moderate impact on the results. The initial oxygen carrier loading is also increased by 50% in MA-CLR because of the added volume of the additional reactor components.

As illustrated in Figure 6, the pressure shell accounts for the bulk of the reactor cost, followed by the reaction vessel and the oxygen carrier. The cost of the insulation material is negligibly small. Figure 6 also indicates that process intensification through pressurization can reduce equipment cost up to a point, after which costs start increasing again. When increasing the pressure from 25 to 50 bar, the

saving from a smaller reactor volume is larger than the added cost of the thicker pressure shell, but this is no longer the case when increasing the pressure further to 100 bar.

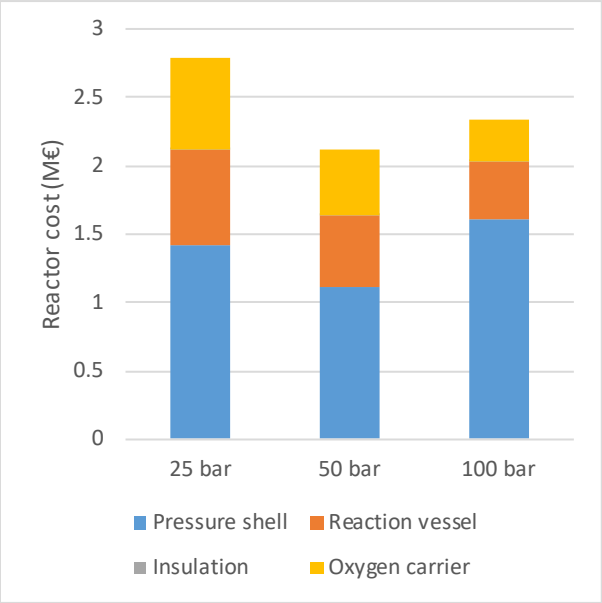

Figure 6: MA-ATR reactor bare module costs for the three reactor pressure levels investigated in this study. The optimal reactor heights calculated via the 1D model at the three pressure levels were 8.1 m, 7.2 m and 6.5 m.

Cost assumptions for the natural gas desulphurization unit [40], pre-reformer [41] and membranes [42] are identical to those of Spallina, Pandolfo [12]. The desulphurization unit and pre-reformer were assumed to cost 0.27 and 2.70 M€ respectively (after cost inflation adjustment via the CEPCI index) for all cases under the assumption that operating pressure does not significantly impact capital costs. Membrane costs were taken as 1000 $/ft^2. Following Spallina, Pandolfo [12], the costs of these units were increased by a 80% to account for installation costs.

Costs of auxiliary facilities (buildings, utilities, etc.) were accounted for by adding 14% to the cost of the gas desulphurization unit, pre-reformer and membranes [12], as well as 50% of the bare module costs under reference conditions (atmospheric pressure and carbon steel material) for all the remaining equipment [39].

Finally, the cost of the fully installed ASU plant supplying the oxygen to the MA-ATR reactor was taken directly from Ebrahimi, Meratizaman [43] as 21 M$ for a plant producing the 2.15-2.2 kg/s of O_2 required by the MA-ATR processes evaluated in this study.

The total installed cost of the plant was then increased by another 18% to account for contingency and fees [39] to give the final cost of the new plant. Annualized capital costs are then calculated as a loan with 10% interest rate over a 25 year plant operating period. Given the wide variability in financing costs, a sensitivity analysis on this interest rate is presented later.

2.3.2 Operating costs

Operating costs are summarized in Table 4. Oxygen carrier lifetimes were assumed as 1 year for MA-CLR and 5 years for MA-ATR because of the much lower attrition losses expected in the gently bubbling MA-ATR reactor compared to the circulating fluidized bed MA-CLR reactor. Membrane lifetime was

assumed to be two years with an 80% cost recovery factor upon replacement due to Pd and support recycling as assumed by Wassie, Cloete [30].

Table 4: Operating cost assumptions from Spallina, Pandolfo [12] unless otherwise indicated.

Fixed operating costs	
Maintenance	2.5% of total capital costs per year
Insurance	2% of total capital costs per year
Labour	€1.5 M€/year
Variable operating costs	
Oxygen carrier	15 $/kg [27]
Cooling water	0.35 €/m^3
Process water	2 €/m^3
Natural gas	6 €/GJ$_{LHV}$ [44]
Steam	1 $/klb [45]
Electricity	60 €/MWh [44]

Natural gas and electricity are the most important variable costs and a sensitivity analysis on the prices of these commodities will be presented later.

2.4 Performance measures

The H_2 production efficiency (η_{H_2}) and equivalent H_2 production efficiency $(\eta_{H_2,eq})$ are defined as follows:

$$\eta_{H_2} = \frac{\dot{m}_{H_2} LHV_{H_2}}{\dot{m}_{NG} LHV_{NG}} \quad \text{Equation 2}$$

$$\eta_{H_2,eq} = \frac{\dot{m}_{H_2} LHV_{H_2}}{\dot{m}_{NG,eq} LHV_{NG}} \quad \text{Equation 3}$$

The equivalent natural gas input $(\dot{m}_{NG,eq})$ used in Equation 3 accounts for exported electricity (W_{el}) assuming an equivalent natural gas power plant efficiency of η_{el}=0.583 and steam with an evaporation enthalpy $h_{evap} = 2.26$ MJ/kg and an equivalent boiler efficiency of $\eta_{th} = 0.9$.

$$\dot{m}_{NG,eq} = \dot{m}_{NG} - \frac{\dot{m}_{steam} h_{evap}}{\eta_{th} LHV_{NG}} - \frac{W_{el}}{\eta_{el} LHV_{NG}} \quad \text{Equation 4}$$

Both MA-ATR and MA-CLR capture 100% of the produced CO_2, but have some indirect emissions dependent on the CO_2 intensity of the consumed electricity. Thus, the CO_2 emissions factor of produced H_2 (g/MJ$_{LHV}$) is defined as follows using a natural gas power plant CO_2 emissions factor of $E_{el} = 97.7$ g/MJ$_{el}$:

$$E_{H_2} = -\frac{W_{el} E_{el}}{\dot{m}_{H_2} LHV_{H_2}} \quad \text{Equation 5}$$

3 Results and discussion

Results will be discussed in four main sections: the effect of reactor pressure, the effect of H_2 permeate pressure, the effect of reactor temperature, and a sensitivity study. All cases are completed with a constant natural gas flowrate of 2.62 kg/s and a steam/carbon ratio of 1.75.

3.1 Effect of reactor pressure

As illustrated in Table 5, MA-ATR generally produces more H_2 than MA-CLR. This increased production is achieved because no heat is required to raise the temperature of N_2 in air to the reactor temperature as in the air reactor of the MA-CLR process. This enables more natural gas to be converted to H_2.

On the other hand, MA-ATR consumes more electricity than MA-CLR and does not produce steam for export. The lack of steam export is of little significance due to the low monetary value of 6 bar saturated steam, but the increased electricity consumption will contribute significant additional costs.

Table 5: Process modelling results for MA-ATR and MA-CLR at different reactor pressures with an H_2 permeation pressure of 1 bar and a reactor temperature of 700 °C.

		25 bar		50 bar		100 bar	
		MA-ATR	MA-CLR	MA-ATR	MA-CLR	MA-ATR	MA-CLR
Natural gas thermal input	MW_{LHV}	121.94	121.94	121.94	121.94	121.94	121.94
H_2 thermal output	MW_{LHV}	114.69	111.24	114.94	111.71	115.24	111.69
Steam thermal output	MW	0.00	0.68	0.00	2.12	0.00	2.98
Net electric power	MW_{el}	-12.86	-11.05	-12.69	-11.02	-12.82	-10.75
Air/ASU compression	MW_{el}	-1.76	-5.06	-1.74	-6.37	-1.72	-7.21
Gas turbine	MW_{el}	0.00	3.70	0.00	4.81	0.00	6.10
ASU O_2 compression	MW_{el}	-0.45	0.00	-0.70	0.00	-1.00	0.00
ASU N_2 compression	MW_{el}	0.00	0.00	0.00	0.00	0.00	0.00
H_2 compression	MW_{el}	-10.05	-9.12	-9.97	-9.22	-9.84	-9.40
CO_2/NG compression	MW_{el}	-0.53	-0.51	-0.18	-0.17	-0.15	-0.15
ASU pumps	MW_{el}	-0.01	0.00	-0.01	0.00	-0.01	0.00
Pumps	MW_{el}	-0.06	-0.06	-0.08	-0.08	-0.10	-0.10
Other auxiliaries	MW_{el}	0.00	0.00	0.00	0.00	0.00	0.00
H_2 mass flow rate	kg/s	0.96	0.93	0.96	0.93	0.96	0.93
Steam export (160 °C, 6 bar)	kg/s	0.00	0.30	0.00	0.94	0.00	1.32
H_2 production efficiency	$H_{2,LHV}/NG_{LHV}$	0.94	0.91	0.94	0.92	0.95	0.92
Eq. H_2 production efficiency	$H_{2,LHV}/NG_{eq,\ LHV}$	0.80	0.79	0.80	0.81	0.80	0.81
CO_2 intensity	g/MJ_{LHV}	10.96	9.70	10.79	9.64	10.87	9.40

Two main reasons can be identified for the increased electricity consumption of MA-ATR. First, the inclusion of the ASU increases power consumption relative to the air compressor and turbine employed in MA-CLR. This difference is not as high as may be expected though. For the 50 bar base case, the net consumption of the ASU and O_2 compression in MA-ATR amounts to 2.45 MW, whereas the MA-CLR compression and turbine have a net consumption of 1.56 MW. Second, the H_2 compressor

consumption in MA-ATR is higher due to the high temperature compression employed to raise the compressed H_2 stream temperature to the level required to produce additional steam. This increased H_2 compressor consumption is 0.75 MW for the base case.

Added electricity consumption also increases effective CO_2 emissions. As shown in Table 5, the CO_2 intensity for H_2 produced via MA-ATR is 1.15 g/MJ higher than MA-CLR. This should be viewed in perspective of natural gas CO_2 intensity of about 55 g/MJ, indicating that the increase in effective CO_2 emissions is small.

The effect of increasing reactor pressure on overall plant performance is essentially negligible. As shown in Figure 7 and Table 6, however, increasing pressure has a significant positive effect on the economics. Higher pressures result in a lower cost of hydrogen for both MA-ATR and MA-CLR, although this positive effect is slightly larger for MA-CLR.

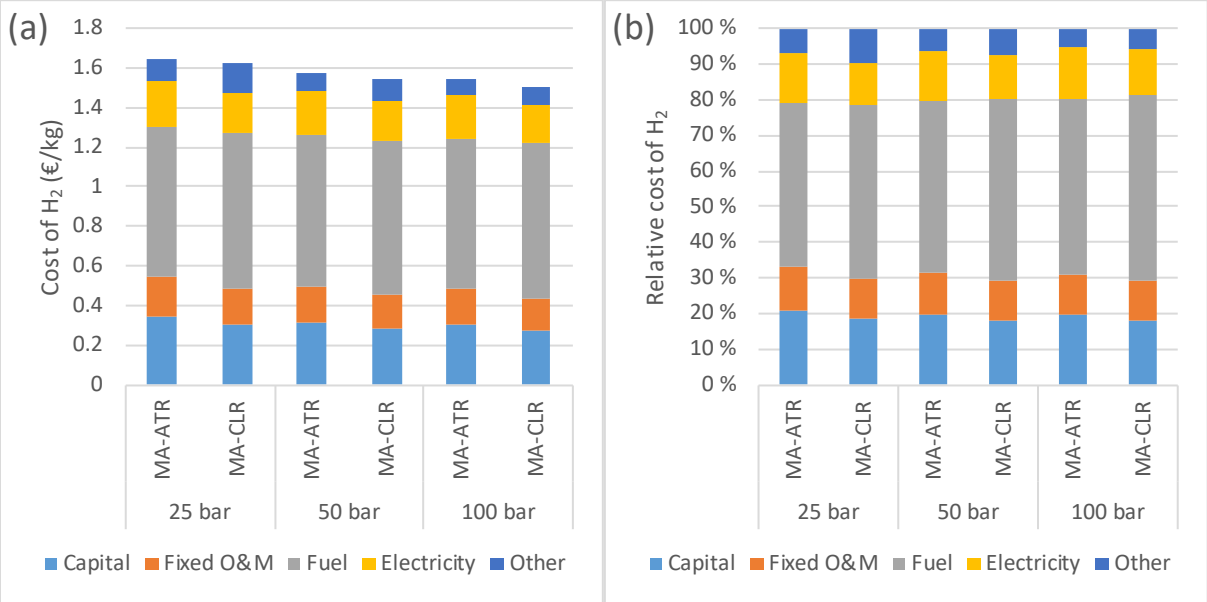

Figure 7: Breakdown of the cost of hydrogen in absolute (a) and relative (b) terms for MA-ATR and MA-CLR at different reactor pressures with an H_2 permeation pressure of 1 bar and a reactor temperature of 700 °C.

Overall, the cost of hydrogen from MA-ATR is slightly higher than from MA-ATR (about 1.5% for the 50 bar case). Compared to MA-CLR, MA-ATR has higher capital costs (mainly because of the ASU), which also leads to higher maintenance costs. Electricity costs are also higher, while natural gas costs are lower due to the higher H_2 production efficiency shown in Table 5. Lastly, oxygen carrier make-up costs are lower due to the higher attrition rate assumed in the circulating fluidized bed MA-CLR reactor.

This small cost increase of MA-ATR relative to MA-CLR implies that MA-ATR remains competitive relative to conventional carbon intensive methods. Spallina, Pandolfo [12] calculated the cost of hydrogen from MA-CLR to be fully 11% lower than that of conventional SMR, so the 1.5% cost increase of MA-ATR does not change its attractiveness relative to current technologies.

Table 6: Economic assessment results for MA-ATR and MA-CLR at different reactor pressures with an H_2 permeation pressure of 1 bar and a reactor temperature of 700 °C.

		25 bar		50 bar		100 bar	
		MA-ATR	MA-CLR	MA-ATR	MA-CLR	MA-ATR	MA-CLR
Reactor height	m	8.1	8.2	7.2	7.1	6.5	6.4
Capital costs							
ASU	M€	17.50	0.00	17.50	0.00	17.50	0.00
Desulphurizer	M€	0.49	0.49	0.49	0.49	0.49	0.49
Pre-reformer	M€	4.86	4.86	4.86	4.86	4.86	4.86
Pumps	M€	0.60	0.50	0.70	0.70	0.75	0.64
H_2 compressors	M€	13.71	12.40	13.57	12.77	13.67	13.05
CO_2 compressors	M€	1.25	1.19	0.52	0.49	0.58	0.36
Air/O_2 turbomachines	M€	0.46	4.22	0.66	5.52	0.86	6.48
Heat exchangers	M€	0.89	0.89	0.86	0.95	0.88	0.96
H_2 coolers	M€	3.18	3.17	3.21	4.34	4.07	4.50
Heat rejection	M€	1.69	2.09	1.82	2.03	1.67	1.62
Reactor	M€	2.23	4.62	2.11	4.07	2.38	4.56
Membranes	M€	17.96	18.64	12.62	12.10	9.28	8.86
Auxiliary facilities	M€	8.73	10.42	7.91	10.30	7.73	10.25
Contingency and fees	M€	11.67	9.55	10.60	8.69	10.26	8.35
Total new plant cost	M€	85.23	73.03	77.42	67.30	74.98	64.98
Annualized capital cost	M€/y	9.39	8.05	8.53	7.41	8.26	7.16
Fixed O&M costs							
Maintenance & insurance	M€/y	3.84	3.29	3.48	3.03	3.37	2.92
Labour	M€/y	1.50	1.50	1.50	1.50	1.50	1.50
Variable O&M costs							
Oxygen carrier	M€/y	0.10	0.77	0.07	0.50	0.05	0.36
Membranes	M€/y	1.80	1.86	1.26	1.21	0.93	0.89
Cooling water	M€/y	0.98	1.15	0.96	0.98	0.97	0.90
Process water	M€/y	0.33	0.33	0.33	0.33	0.33	0.33
Natural gas	M€/y	20.77	20.77	20.77	20.77	20.77	20.77
Steam export	M€/y	0.00	-0.02	0.00	-0.05	0.00	-0.07
Electricity	M€/y	6.08	5.23	6.00	5.21	6.07	5.08
Total annual cost	M€/y	44.78	42.92	42.90	40.89	42.25	39.85
Cost of hydrogen	€/kg	1.65	1.63	1.58	1.55	1.55	1.51

3.2 Effect of H_2 permeate pressure

Table 7 shows that increasing the permeate pressure significantly increases the equivalent H_2 production efficiency by reducing the power consumption of the H_2 compressors. This effect is similar for both the MA-ATR and MA-CLR concepts.

As shown in Figure 8 and Table 8, however, this increased efficiency brings a trade-off in terms of higher reactor and membrane costs. When increasing the H_2 permeation pressure from 1 bar to 2 bar, the increased reactor and membrane costs are largely cancelled out by lower costs of H_2 compressors and coolers, but this is no longer the case when further increasing the H_2 permeation pressure to 4 bar.

Table 7: Process modelling results for MA-ATR and MA-CLR at different H_2 permeation pressures with reactor pressure of 50 bar and a reactor temperature of 700 °C.

		1 bar		2 bar		4 bar	
		MA-ATR	MA-CLR	MA-ATR	MA-CLR	MA-ATR	MA-CLR
Natural gas thermal input	MW_{LHV}	121.94	121.94	121.94	121.94	121.94	121.94
H_2 thermal output	MW_{LHV}	114.94	111.71	114.94	111.71	114.94	111.71
Steam thermal output	MW	0.00	2.12	0.00	2.12	0.00	2.12
Net electric power	MW_{el}	-12.69	-11.02	-11.31	-9.59	-10.00	-8.26
Air/ASU compression	MW_{el}	-1.74	-6.37	-1.74	-6.37	-1.74	-6.37
Gas turbine	MW_{el}	0.00	4.81	0.00	4.81	0.00	4.81
ASU O_2 compression	MW_{el}	-0.70	0.00	-0.70	0.00	-0.70	0.00
ASU N_2 compression	MW_{el}	0.00	0.00	0.00	0.00	0.00	0.00
H_2 compression	MW_{el}	-9.97	-9.22	-8.59	-7.79	-7.28	-6.45
CO_2/NG compression	MW_{el}	-0.18	-0.17	-0.18	-0.17	-0.18	-0.17
ASU pumps	MW_{el}	-0.01	0.00	-0.01	0.00	-0.01	0.00
Pumps	MW_{el}	-0.08	-0.08	-0.08	-0.08	-0.08	-0.08
Other auxiliaries	MW_{el}	0.00	0.00	0.00	0.00	0.00	0.00
H_2 mass flow rate	kg/s	0.96	0.93	0.96	0.93	0.96	0.93
Steam export (160 °C, 6 bar)	kg/s	0.00	0.94	0.00	0.94	0.00	0.94
H_2 production efficiency	$H_{2,LHV}/NG_{LHV}$	0.94	0.92	0.94	0.92	0.94	0.92
Eq. H_2 production efficiency	$H_{2,LHV}/NG_{eq,\ LHV}$	0.80	0.81	0.81	0.82	0.83	0.84
CO_2 intensity	g/MJ_{LHV}	0.12	0.09	0.10	0.08	0.09	0.06

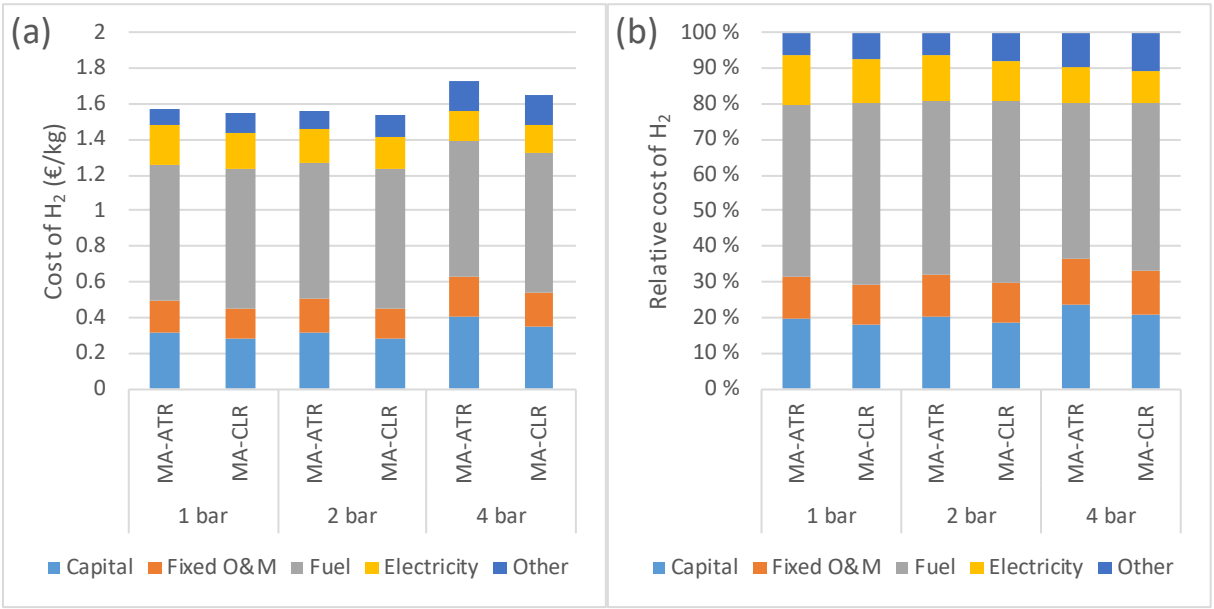

Figure 8: Breakdown of the cost of hydrogen in absolute (a) and relative (b) terms for MA-ATR and MA-CLR at different H_2 permeation pressures with a reactor pressure of 50 bar and a reactor temperature of 700 °C.

In the 4 bar case, the H_2 partial pressure in the upper regions of the reactor approaches the pressure inside the membranes, resulting in a greatly reduced H_2 flux and a large increase in the required membrane surface area (and hence also the reactor volume). Here, the slightly larger amount of fuel combustion required in MA-CLR has a significant effect by allowing the H_2 partial pressure in the upper membrane regions to be slightly higher than for MA-ATR, creating a relatively large increase in H_2 flux through the membranes.

Table 8: Economic assessment results for MA-ATR and MA-CLR at different H_2 permeation pressures with a reactor pressure of 50 bar and a reactor temperature of 700 °C.

		1 bar		2 bar		4 bar	
		MA-ATR	MA-CLR	MA-ATR	MA-CLR	MA-ATR	MA-CLR
Reactor height	m	7.2	7.1	7.7	7.6	9.8	9.1
Capital costs							
ASU	M€	17.50	0.00	17.50	0.00	17.50	0.00
Desulphurizer	M€	0.49	0.49	0.49	0.49	0.49	0.49
Pre-reformer	M€	4.86	4.86	4.86	4.86	4.86	4.86
Pumps	M€	0.70	0.70	0.72	0.61	0.65	0.61
H_2 compressors	M€	13.57	12.77	12.21	11.45	10.77	10.08
CO_2 compressors	M€	0.52	0.49	0.52	0.49	0.52	0.49
Air/O_2 turbomachines	M€	0.66	5.52	0.66	5.52	0.66	5.52
Heat exchangers	M€	0.86	0.95	0.86	0.95	0.85	0.95
H_2 coolers	M€	3.21	4.34	2.38	3.11	1.75	2.40
Heat rejection	M€	1.82	2.03	1.68	1.84	1.60	1.75
Reactor	M€	2.11	4.07	2.55	4.92	5.19	8.30
Membranes	M€	12.62	12.10	15.43	14.84	31.82	25.47
Auxiliary facilities	M€	7.91	10.30	7.74	10.04	9.55	11.09
Contingency and fees	M€	10.60	8.69	10.78	8.83	13.80	10.97
Total new plant cost	M€	77.42	67.30	78.38	67.94	99.99	82.97
Annualized capital cost	M€/y	8.53	7.41	8.64	7.48	11.02	9.14
Fixed O&M costs							
Maintenance & insurance	M€/y	3.48	3.03	3.53	3.06	4.50	3.73
Labour	M€/y	1.50	1.50	1.50	1.50	1.50	1.50
Variable O&M costs							
Oxygen carrier	M€/y	0.07	0.50	0.08	0.61	0.17	1.05
Membranes	M€/y	1.26	1.21	1.54	1.48	3.18	2.55
Cooling water	M€/y	0.96	0.98	0.85	0.87	0.75	0.77
Process water	M€/y	0.33	0.33	0.33	0.33	0.33	0.33
Natural gas	M€/y	20.77	20.77	20.77	20.77	20.77	20.77
Steam export	M€/y	0.00	-0.05	0.00	-0.05	0.00	-0.05
Electricity	M€/y	6.00	5.21	5.35	4.54	4.73	3.91
Total annual cost	M€/y	42.90	40.89	42.59	40.59	46.95	43.69
Cost of hydrogen	€/kg	1.58	1.55	1.56	1.53	1.72	1.65

As a result of these capital cost dynamics, the cost of hydrogen decreases from 1 bar to 2 bar permeate pressure as capital costs remain similar, but electricity costs reduce. When increasing the permeate

pressure to 4 bar, however, a large increase in capital cost cancels out the further reduction in electricity cost for both MA-ATR and MA-CLR.

3.3 Effect of reactor temperature

Table 9 shows that an increase in reactor temperature results in less power consumption at the expense of less H_2 production, particularly for the MA-CLR case. Higher reactor temperatures require more fuel to be combusted to raise the temperature of the incoming gases to the reactor temperature. In MA-CLR, this results in more energy being available in the air reactor outlet gas for power generation (see the increase in the gas turbine output with an increase in reactor temperature in Table 9).

For MA-ATR, a reduction in temperature from 700 °C to 600 °C did not significantly change the H_2 production or electricity consumption of the plant. This is because the reactor inlet stream had to be cooled to raise additional steam. Thus, the effect of the lower outlet temperature in the 600 °C case is cancelled out by a lower inlet temperature. However, in the 800 °C case, the electricity consumption reduces as more heat becomes available for steam generation from the reactor outlet streams, requiring less high temperature H_2 compression to generate additional heat for raising steam.

Overall, this trade-off between H_2 production and electricity consumption causes the H_2 production efficiency to decline with increasing temperature, but the equivalent H_2 production efficiency to stay constant (Table 9).

Table 9: Process modelling results for MA-ATR and MA-CLR at different reactor temperatures with a reactor pressure of 50 bar and a permeate pressure of 1 bar.

		600 °C		700 °C		800 °C	
		MA-ATR	MA-CLR	MA-ATR	MA-CLR	MA-ATR	MA-CLR
Natural gas thermal input	MW_{LHV}	121.94	121.94	121.94	121.94	121.94	121.94
H_2 thermal output	MW_{LHV}	115.07	115.56	114.94	111.71	112.18	107.44
Steam thermal output	MW	0.00	0.00	0.00	2.12	0.00	4.51
Net electric power	MW_{el}	-12.70	-12.71	-12.69	-11.02	-12.08	-10.08
Air/ASU compression	MW_{el}	-1.74	-6.37	-1.74	-6.37	-1.74	-6.37
Gas turbine	MW_{el}	0.00	4.30	0.00	4.81	0.00	5.36
ASU O_2 compression	MW_{el}	-0.70	0.00	-0.70	0.00	-0.70	0.00
ASU N_2 compression	MW_{el}	0.00	0.00	0.00	0.00	0.00	0.00
H_2 compression	MW_{el}	-9.98	-10.39	-9.97	-9.22	-9.36	-8.82
CO_2/NG compression	MW_{el}	-0.18	-0.17	-0.18	-0.17	-0.18	-0.17
ASU pumps	MW_{el}	-0.01	0.00	-0.01	0.00	-0.01	0.00
Pumps	MW_{el}	-0.08	-0.08	-0.08	-0.08	-0.08	-0.08
Other auxiliaries	MW_{el}	0.00	0.00	0.00	0.00	0.00	0.00
H_2 mass flow rate	kg/s	0.96	0.96	0.96	0.93	0.94	0.90
Steam export (160 °C, 6 bar)	kg/s	0.00	0.00	0.00	0.94	0.00	2.16
H_2 production efficiency	$H_{2,LHV}/NG_{LHV}$	0.94	0.95	0.94	0.92	0.92	0.88
Eq. H_2 production efficiency	$H_{2,LHV}/NG_{eq,\ LHV}$	0.80	0.80	0.80	0.81	0.79	0.80
CO_2 intensity	g/MJ_{LHV}	0.12	0.12	0.12	0.09	0.11	0.07

Regarding economics, a significant positive effect of higher reactor temperatures is observed in Figure 9. As can be seen in Table 10, this improvement is due almost entirely to the lower membrane surface area and smaller reactor size facilitated by an increase in reactor temperature, with membrane cost easily being the most important factor. As the temperature increases, the H_2 concentration increases because the steam methane reforming reaction is thermodynamically favoured at higher temperatures. This increases the driving force for H_2 permeation.

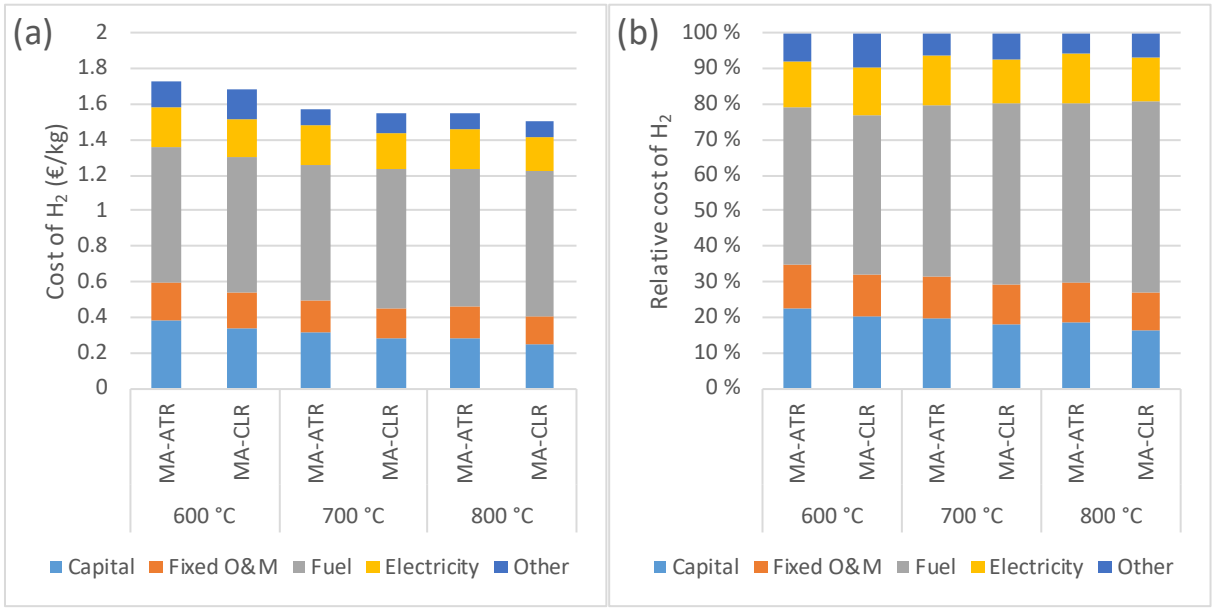

Figure 9: Breakdown of the cost of hydrogen in absolute (a) and relative (b) terms for MA-ATR and MA-CLR at different reactor temperatures with a reactor pressure of 50 bar and a permeate pressure of 1 bar.

As could be anticipated from the results in Table 9, there is a trade-off between fuel costs and electricity costs: higher reactor temperatures increase fuel costs and lower electricity costs. Note that, although natural gas costs are kept constant in Table 10, the amount of H_2 produced from the constant fuel input decreases with increased temperature (Table 9), causing an increase in fuel costs per unit H_2 produced.

The large increase in membrane cost when reducing the temperature from 700 to 600 °C is important because the long-term stability and permeability of Pd-based H_2 membranes can degrade rapidly if the temperature becomes too high. Although some Pd-membranes have been successfully operated in longer-term tests at 650 °C [46, 47], several studies reported challenges at higher temperatures as summarized in the review by Gallucci, Medrano [48]. However, given the ongoing research and initial commercialization efforts of Pd membranes, it can be reasonably expected that the central case at 700 °C will become practically feasible as H_2 membrane science matures.

Table 10: Economic assessment results for MA-ATR and MA-CLR at reactor temperatures with a reactor pressure of 50 bar and a permeate pressure of 1 bar.

		600 °C		700 °C		800 °C	
		MA-ATR	MA-CLR	MA-ATR	MA-CLR	MA-ATR	MA-CLR
Reactor height	m	9.0	8.8	7.7	7.6	6.3	6.3
Capital costs							
ASU	M€	17.50	0.00	17.50	0.00	17.50	0.00
Desulphurizer	M€	0.49	0.49	0.49	0.49	0.49	0.49
Pre-reformer	M€	4.86	4.86	4.86	4.86	4.86	4.86
Pumps	M€	0.65	0.59	0.70	0.70	0.73	0.59
H_2 compressors	M€	13.58	13.77	13.57	12.77	12.75	11.36
CO_2 compressors	M€	0.52	0.48	0.52	0.49	0.52	0.48
Air/O_2 turbomachines	M€	0.66	5.49	0.66	5.52	0.66	5.54
Heat exchangers	M€	0.95	0.84	0.86	0.95	0.89	1.63
H_2 coolers	M€	3.03	3.30	3.21	4.34	1.94	2.04
Heat rejection	M€	1.82	1.88	1.82	2.03	2.15	2.07
Reactor	M€	4.02	7.51	2.11	4.07	1.47	2.94
Membranes	M€	24.64	23.04	12.62	12.10	8.45	8.45
Auxiliary facilities	M€	9.60	11.84	7.91	10.30	6.86	9.06
Contingency and fees	M€	13.09	11.20	10.60	8.69	9.43	7.28
Total new plant cost	M€	95.38	85.29	77.42	67.30	68.69	56.79
Annualized capital cost	M€/y	10.51	9.40	8.53	7.41	7.57	6.26
Fixed O&M costs							
Maintenance & insurance	M€/y	4.29	3.84	3.48	3.03	3.09	2.56
Labour	M€/y	1.50	1.50	1.50	1.50	1.50	1.50
Variable O&M costs							
Oxygen carrier	M€/y	0.14	0.95	0.07	0.50	0.05	0.35
Membranes	M€/y	2.46	2.30	1.26	1.21	0.85	0.85
Cooling water	M€/y	0.96	0.99	0.96	0.98	1.18	1.07
Process water	M€/y	0.33	0.33	0.33	0.33	0.33	0.33
Natural gas	M€/y	20.77	20.77	20.77	20.77	20.77	20.77
Steam export	M€/y	0.00	0.00	0.00	-0.05	0.00	-0.05
Electricity	M€/y	6.01	6.01	6.00	5.21	5.72	4.77
Total annual cost	M€/y	46.96	46.08	42.90	40.89	41.04	38.39
Cost of hydrogen	€/kg	1.72	1.68	1.58	1.55	1.54	1.51

Reactor temperatures of 800 °C may be out of reach for Pd membranes, but this analysis shows that limited economic benefits can be derived from an increase in reactor temperature from 700 to 800 °C. A maximum operating temperature of 700 °C therefore appears to be a good target for membrane development for the MA-ATR and MA-CLR concepts.

However, despite the 9% increase in the cost of hydrogen when decreasing the reactor temperature from 700 to 600 °C, the MA-ATR concept will still be highly attractive when a meaningful CO_2 price is

introduced. However, temperatures of 650-700 °C will be required to ensure economic attractiveness in an environment with no price on CO_2 [12].

3.4 Sensitivity analysis

The sensitivity of MA-ATR and MA-CLR economics to four key parameters is illustrated in Figure 10. Firstly, the uncertainties related to reactor costing are explored. Given that pressurized chemical looping is still at the small scale demonstration phase with relatively low operating pressures, it is highly uncertain what a large-scale MA-CLR reactor operating at 50 bar will cost. This is explored in Figure 10a by varying the cost multiple of the MA-CLR reactor over the MA-ATR reactor between values of 1 and 5. Uncertainty also exists about the cost of the simpler MA-ATR reactor, so this cost is varied between -50% to +100% of the base value.

As illustrated in Figure 10a, the MA-ATR reactor cost variation only causes 1.4% of variation in the cost of hydrogen, making this uncertainty insignificant in the cost estimation. For MA-CLR, the change in cost assumptions causes 8.6% variation, which is significant, but not large enough to change the conclusions about the attractiveness of the MA-CLR technology. Successful scale-up and deployment of MA-CLR will therefore be determined by technical challenges related to high pressure chemical looping rather than reactor costs.

Figure 10b shows a substantial impact of financing costs on the cost of hydrogen. Still, Figure 7b and Figure 8b show that capital costs only account for ~20% of the cost of hydrogen with a 10% interest rate, so capital is not a main determining factor of MA-ATR or MA-CLR process economics. MA-ATR is slightly more capital-intensive than MA-CLR, making it more sensitive to financing costs.

The impact of membrane costs is shown in Figure 10c to have an effect of similar magnitude to that of financing costs. Sensitivities are provided for the three different reactor pressures to illustrate the lower sensitivity at higher reactor pressures where the required membrane surface area is reduced. In general, if the reactor is operated at the maximum achievable pressure, which improves the economics of both processes, the sensitivity to membrane costs becomes quite low. This conclusion extends to other membrane-related assumptions such as lifetime and cost recovery factors.

Finally, Figure 10d illustrates the sensitivity to the prices of energy inputs in terms of natural gas and electricity. Figure 7b and Figure 8b show that fuel represents the dominant component in the cost of hydrogen from both processes, so it is not surprising that process economics are highly sensitive to the natural gas price. Given that MA-ATR has a slightly higher H_2 production efficiency than MA-CLR, it is slightly less sensitive to the natural gas price. MA-ATR uses more electricity, however, making it more sensitive to the electricity price.

These differences between the two processes are subtle though. In the extreme of high natural gas and low electricity prices, MA-ATR returns the same cost of hydrogen as MA-CLR. On the other extreme of low natural gas prices and high electricity prices, MA-ATR is only 5% more expensive than MA-CLR. Given that electricity prices are influenced by natural gas prices, this difference in sensitivity to energy input prices between MA-ATR and MA-CLR is not of high importance.

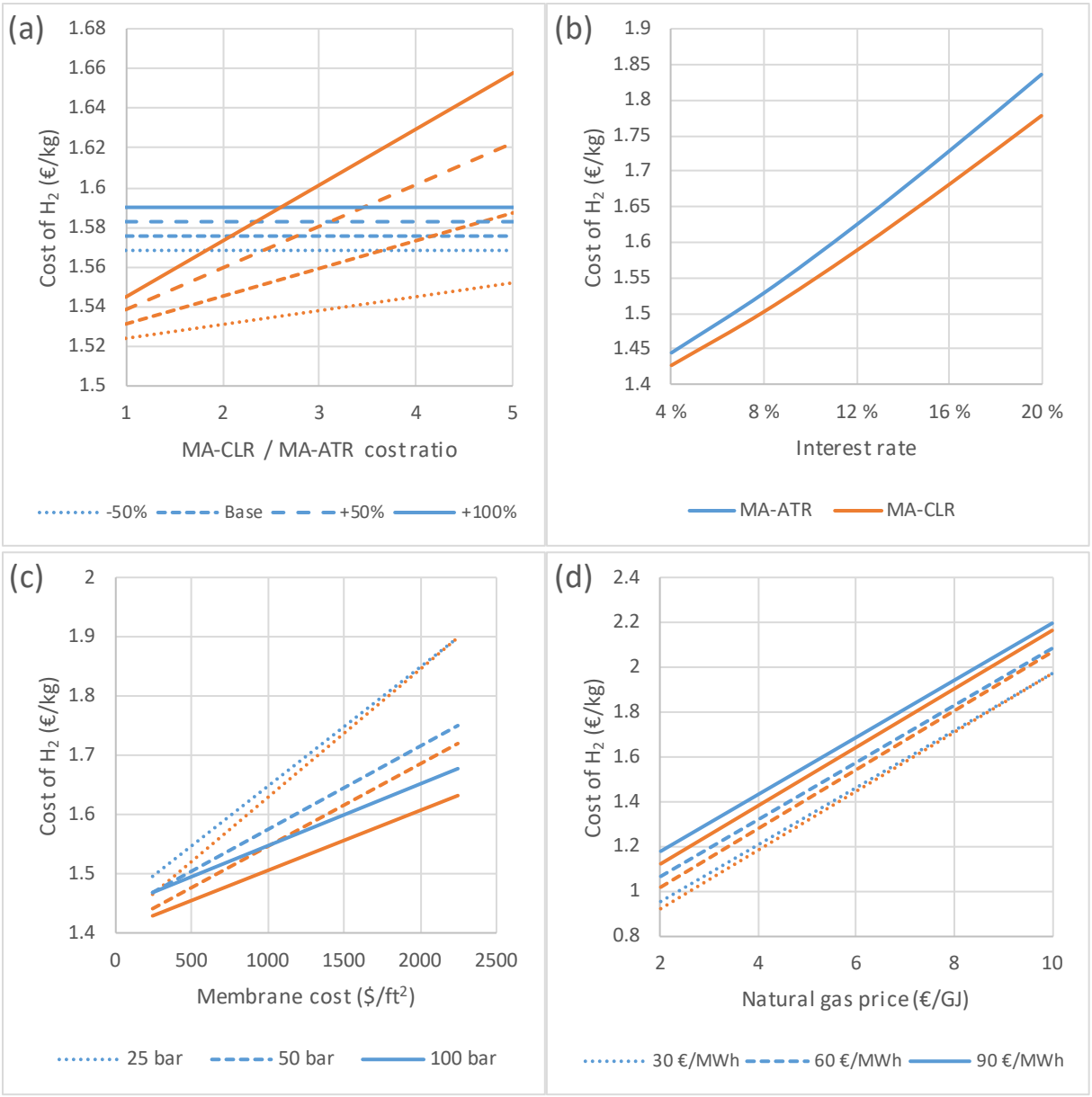

Figure 10: Sensitivity of the cost of hydrogen to reactor cost assumptions (a), financing costs (b), membrane costs (c), and fuel & electricity prices (d). In all cases, blue lines represent MA-ATR and orange lines represent MA-CLR.

4 Summary and conclusions

Membrane-assisted autothermal reforming (MA-ATR) uses a single high-pressure bubbling fluidized bed reactor to convert natural gas to high purity hydrogen with 100% CO_2 capture. The reactor operates by employing H_2 perm-selective membranes in the lower reactor regions to extract H_2 produced by steam methane reforming over the Ni-based fluidized catalyst particles. Above the membranes, high purity O_2 from an air separation unit (ASU) is injected to oxidize the Ni-based oxygen carrier material so that it can react with the fuel gases slipping past the membranes to enable autothermal operation. The good mixing in the fluidized bed then distributes the produced heat to the lower reactor regions to drive the endothermic reforming reactions.

The MA-ATR concept was inspired by the excellent economic performance reported for the membrane assisted chemical looping reforming (MA-CLR) process evaluated by Spallina, Pandolfo [12]. MA-ATR is

proposed to avoid the technical challenge of achieving reliable solids circulation between large-scale MA-CLR air and fuel reactors under the high operating pressures (>50 bar) required for good process economics.

The economic assessment showed that MA-ATR can replicate the performance of MA-CLR for costs that are only 1.5% higher in the base case. Even though the inclusion of an ASU significantly increases capital costs and electricity consumption, these added costs are largely offset by an increased H_2 production efficiency (because additional fuel combustion to heat air in the MA-CLR air reactor is not required), avoidance of turbomachinery for compressing and expanding air to the air reactor, and lower reactor costs.

Reactor costs are an important uncertainty in this analysis, but changes to the reactor cost assumptions had a negligible effect on the MA-ATR assessment and only a moderate effect on the MA-CLR assessment. Other sensitivities to financing costs, membrane costs, fuel and electricity prices are larger and very similar between MA-ATR and MA-CLR.

It can therefore be concluded that MA-ATR is an attractive alternative to MA-CLR, depending on the technical challenges of achieving reliable chemical looping operation in large scale reactors operating at 50 bar or higher. If the scale-up of pressurized chemical looping technology continues at the current slow pace, MA-ATR offers an attractively simple reactor concept that will, similar to MA-CLR, be able to compete with conventional carbon-intensive H_2 production pathways without CO_2 pricing.

Future work should focus on testing the long-term performance and reliability of membranes under industrially relevant pressures and temperatures. The economics of MA-ATR continue to improve as reactor pressure and temperature are increased, both of which will put increasing stresses on the membranes. If membrane longevity under 50 bar pressure and 650-700 °C temperature can be proven, MA-ATR could be scaled up rapidly and deployed for cost-competitive clean H_2 production.

5 Acknowledgement

The authors gratefully acknowledge the funding from Gassnova under the CLIMIT idea development call (project number: 618121).

6 Nomenclature

AR	Air reactor
ASU	Air separation unit
CEPCI	Chemical engineering plant cost index
CLC	Chemical looping combustion
CLR	Chemical looping reforming
ECO	Economizer
EVA	Evaporator

FR	Fuel reactor
HE	Heat exchanger
HP	High pressure
LP	Low pressure
MA-ATR	Membrane assisted autothermal reforming
MA-CLR	Membrane assisted chemical looping reforming
MHE	Main heat exchanger
NG	Natural gas
OC	Oxygen carrier
O&M	Operating and maintenance
R&D	Research and development
SH	Superheater
SMR	Steam methane reforming
TSA	Temperature swing adsorption
WGS	Water-gas shift

7 Appendix

Table 11 and Table 12 report the stream data at the selected locations in both plants for the base case: reforming temperature of 700 °C and at 50/1 bar retentate/permeate pressure.

Table 11: Stream thermodynamic conditions at the selected locations represented in Figure 2.

Point	T	P	Mass flow	Mole composition (%)							
	°C	bar	kg/s	CH_4	C_{2+}	N_2	O_2	CO_2	H_2O	H_2	Ar
1	15	70	2.62	89	8.11	0.89	0	2	0	0	0
2	324	70	2.62	89	8.11	0.89	0	2	0	0	0
3	490	50.5	7.51	31.64	2.23	0.31	0	0.70	65.12	0.00	0
4	454	50	7.51	33.41	0	0.30	0	2.80	58.07	5.42	0
5	700	49.5	9.01	0	0	0.5	0	57.8	41.3	0.2	0
6	365	49.5	9.01	0	0	0.5	0	57.8	41.3	0.2	0
7	30	110	6.98	0	0	0.85	0	98.35	0.12	0.34	0
8	15	1	10.49	0	0	77.4	20.8	0	1	0	0.8
9	500	50	10.49	0	0	77.4	20.8	0	1	0	0.8
10	900	49.5	8.08	0	0	97.6	0	0	1.2	0	1.2
11	641	49.5	8.08	0	0	97.6	0	0	1.2	0	1.2
12	85	1	8.08	0	0	97.6	0	0	1.2	0	1.2

13	700	1	0.93	0	0	0	0	0	0	100	0
14	179	1	0.93	0	0	0	0	0	0	100	0
15	178	1	0.93	0	0	0	0	0	0	100	0
16	276	1.82	0.93	0	0	0	0	0	0	100	0
17	179	1.82	0.93	0	0	0	0	0	0	100	0
18	30	150	0.93	0	0	0	0	0	0	100	0
19	15	1	4.89	0	0	0	0	0	100	0	0
20	260	51.5	4.89	0	0	0	0	0	100	0	0
21	275	51.5	3.35	0	0	0	0	0	100	0	0
22	275	50.5	1.40	0	0	0	0	0	100	0	0
23	275	50.5	1.54	0	0	0	0	0	100	0	0
24	15	1	0.94	0	0	0	0	0	100	0	0
25	170	6	0.94	0	0	0	0	0	100	0	0

Table 12: Stream thermodynamic condition at the selected locations represented in Figure 3

Point	T	P	Mass flow	Mole composition (%)							
	°C	bar	kg/s	CH_4	C_{2+}	N_2	O_2	CO_2	H_2O	H_2	Ar
1	15	70	2.62	89	8.11	0.89	0	2	0	0	0
2	324	70	2.62	89	8.11	0.89	0	2	0	0	0
3	440	51	7.51	31.64	2.23	0.31	0	0.70	65.12	0.00	0
4	456	50	7.51	34.09	0	0.30	0	2.42	59.36	3.84	0
5	700	49.5	8.91	0	0	1.88	0	60.49	37.62	0	0
6	354	49.5	8.91	0	0	1.88	0	60.49	37.62	0	0
7	30	110	7.13	0	0	3.01	0	96.87	0.12	0	0
8	15	1.0	9.70	0	0	77.30	20.74	0.03	1.01	0	0.92
9	13	4.7	2.34	0	0	1.19	95.12	0	0	0	3.70
10	326	50	2.34	0	0	1.19	95.12	0	0	0	3.70
11	700	1.0	0.96	0	0	0	0	0	0	100	0
12	201	1.0	0.96	0	0	0	0	0	0	100	0
13	412	3.2	0.96	0	0	0	0	0	0	100	0
14	201	3.2	0.96	0	0	0	0	0	0	100	0
15	30	150	0.96	0	0	0	0	0	0	100	0
16	15	1	4.89	0	0	0	0	0	100	0	0
17	260	52	4.89	0	0	0	0	0	100	0	0
18	275	52	4.60	0	0	0	0	0	100	0	0
19	260	52	0.29	0	0	0	0	0	100	0	0
20	275	52	0.29	0	0	0	0	0	100	0	0

8 References

1. IPCC, *Fifth assessment report: Mitigation of climate change*. 2014, Intergovernmental panel on Climate Change.
2. UNFCCC. *Historic Paris Agreement on Climate Change*. United Nations Framework Convention on Climate Change 2015; Available from: https://unfccc.int/process-and-meetings/the-paris-agreement/the-paris-agreement.

3. da Silva Veras, T., et al., *Hydrogen: Trends, production and characterization of the main process worldwide.* International Journal of Hydrogen Energy, 2017. **42**(4): p. 2018-2033.
4. Nikolaidis, P. and A. Poullikkas, *A comparative overview of hydrogen production processes.* Renewable and Sustainable Energy Reviews, 2017. **67**: p. 597-611.
5. Dincer, I. and C. Acar, *Review and evaluation of hydrogen production methods for better sustainability.* International Journal of Hydrogen Energy, 2015. **40**(34): p. 11094-11111.
6. Khojasteh Salkuyeh, Y., B.A. Saville, and H.L. MacLean, *Techno-economic analysis and life cycle assessment of hydrogen production from natural gas using current and emerging technologies.* International Journal of Hydrogen Energy, 2017. **42**(30): p. 18894-18909.
7. Rydén, M., A. Lyngfelt, and T. Mattisson, *Synthesis gas generation by chemical-looping reforming in a continuously operating laboratory reactor.* Fuel, 2006. **85**(12–13): p. 1631-1641.
8. Pröll, T., *Syngas and a separate nitrogen/argon stream via chemical looping reforming-A 140 kW pilot plant study.* Fuel, 2009.
9. Lyngfelt, A., B. Leckner, and T. Mattisson, *A fluidized-bed combustion process with inherent CO2 separation; Application of chemical-looping combustion.* Chemical Engineering Science, 2001. **56**(10): p. 3101-3113.
10. Ishida, M., D. Zheng, and T. Akehata, *Evaluation of a chemical-looping-combustion power-generation system by graphic exergy analysis.* Energy, 1987. **12**(2): p. 147-154.
11. Medrano, J.A., et al., *Thermodynamic analysis of a membrane-assisted chemical looping reforming reactor concept for combined H2 production and CO2 capture.* International Journal of Hydrogen Energy, 2014. **39**(9): p. 4725-4738.
12. Spallina, V., et al., *Techno-economic assessment of membrane assisted fluidized bed reactors for pure H2 production with CO2 capture.* Energy Conversion and Management, 2016. **120**: p. 257-273.
13. Gallucci, F., M. Van Sint Annaland, and J.A.M. Kuipers, *Autothermal Reforming of Methane with Integrated CO2 Capture in a Novel Fluidized Bed Membrane Reactor. Part 2 Comparison of Reactor Configurations.* Topics in Catalysis, 2008. **51**(1): p. 146.
14. Gallucci, F., et al., *Steam Reforming of Methane in a Membrane Reactor: An Industrial Case Study.* Industrial & Engineering Chemistry Research, 2006. **45**(9): p. 2994-3000.
15. Patel, K.S. and A.K. Sunol, *Modeling and simulation of methane steam reforming in a thermally coupled membrane reactor.* International Journal of Hydrogen Energy, 2007. **32**(13): p. 2344-2358.
16. Gallucci, F., M. Van Sintannaland, and J.A.M. Kuipers, *Theoretical comparison of packed bed and fluidized bed membrane reactors for methane reforming.* International Journal of Hydrogen Energy, 2010. **35**(13): p. 7142-7150.
17. Gallucci, F., et al., *Recent advances on membranes and membrane reactors for hydrogen production.* Chemical Engineering Science, 2013. **92**(0): p. 40-66.
18. Gallucci, F., M. Van Sint Annaland, and J.A.M. Kuipers, *Autothermal Reforming of Methane with Integrated CO2 Capture in a Novel Fluidized Bed Membrane Reactor. Part 1: Experimental Demonstration.* Topics in Catalysis, 2008. **51**(1): p. 133.
19. Andrés, M.-B., et al., *In-situ CO2 capture in a pilot-scale fluidized-bed membrane reformer for ultra-pure hydrogen production.* International Journal of Hydrogen Energy, 2011. **36**(6): p. 4038-4055.
20. Roses, L., et al., *Experimental study of steam methane reforming in a Pd-based fluidized bed membrane reactor.* Chemical Engineering Journal, 2013. **222**: p. 307-320.
21. Medrano, J.A., et al., *Pd-based metallic supported membranes: High-temperature stability and fluidized bed reactor testing.* International Journal of Hydrogen Energy, 2016. **41**(20): p. 8706-8718.
22. Wassie, S.A., et al., *Hydrogen production with integrated CO2 capture in a membrane assisted gas switching reforming reactor: Proof-of-Concept.* International Journal of Hydrogen Energy, 2018. **43**(12): p. 6177-6190.

23. Wang, S., et al., *Chemical looping combustion of coke oven gas by using Fe2O3/CuO with MgAl2O4 as oxygen carrier.* Energy & Environmental Science, 2010. **3**(9): p. 1353-1360.
24. Song, T., et al., *Evaluation of hematite oxygen carrier in chemical-looping combustion of coal.* Fuel, 2013. **104**: p. 244-252.
25. Mahecha-Botero, A., et al., *Pure hydrogen generation in a fluidized-bed membrane reactor: Experimental findings.* Chemical Engineering Science, 2008. **63**(10): p. 2752-2762.
26. Mahecha-Botero, A., et al., *Pure hydrogen generation in a fluidized bed membrane reactor: Application of the generalized comprehensive reactor model.* Chemical Engineering Science, 2009. **64**(17): p. 3826-3846.
27. Adanez, J., et al., *Progress in Chemical-Looping Combustion and Reforming technologies.* Progress in Energy and Combustion Science, 2012. **38**(2): p. 215-282.
28. Fu, C. and T. Gundersen, *Recuperative vapor recompression heat pumps in cryogenic air separation processes.* Energy, 2013. **59**: p. 708-718.
29. Stull, D.R. and H. Prophet, *JANAF Thermochemical Tables, 2nd edition*, in *U.S. National Bureau of Standards*. 1971: Washington D.C.
30. Wassie, S.A., et al., *Techno-economic assessment of membrane-assisted gas switching reforming for pure H2 production with CO2 capture.* International Journal of Greenhouse Gas Control, 2018. **72**: p. 163-174.
31. Xu, J. and G.F. Froment, *Methane steam reforming, methanation and water-gas shift: I. Intrinsic kinetics.* AIChE Journal, 1989. **35**(1): p. 88-96.
32. Oliveira, E.L.G., C.A. Grande, and A.E. Rodrigues, *Methane steam reforming in large pore catalyst.* Chemical Engineering Science, 2010. **65**(5): p. 1539-1550.
33. Abad, A., et al., *Mapping of the range of operational conditions for Cu-, Fe-, and Ni-based oxygen carriers in chemical-looping combustion.* Chemical Engineering Science, 2007. **62**(1-2): p. 533-549.
34. Fernandez, E., et al., *Preparation and characterization of metallic supported thin Pd–Ag membranes for hydrogen separation.* Chemical Engineering Journal, 2016. **305**: p. 182-190.
35. Lee, G.S. and S.D. Kim, *Axial mixing of solids in turbulent fluidized beds.* The Chemical Engineering Journal, 1990. **44**(1): p. 1-9.
36. Igci, Y., et al., *Filtered two-fluid models for fluidized gas-particle suspensions.* AIChE Journal, 2008. **54**(6): p. 1431-1448.
37. Holloway, W. and S. Sundaresan, *Filtered models for reacting gas–particle flows.* Chemical Engineering Science, 2012. **82**(0): p. 132-143.
38. Morgado, J.F., et al., *1D modelling of membrane-assisted chemical looping reforming.* Energy Procedia, 2017. **136**: p. 277-282.
39. Turton, R., et al., *Analysis, synthesis and design of chemical processes: Appendix A*. 2008: Pearson Education.
40. Gazzani, M., E. Macchi, and G. Manzolini, *CO2 capture in natural gas combined cycle with SEWGS. Part A: Thermodynamic performances.* International Journal of Greenhouse Gas Control, 2013. **12**: p. 493-501.
41. Manzolini, G., et al., *Technical Economic Evaluation of a System for Electricity Production With CO2 Capture Using a Membrane Reformer With Permeate Side Combustion.* 2006(42398): p. 89-99.
42. Acquaviva, J., *High-Performance, Durable, Palladium Alloy Membrane for Hydrogen Separation and Purification*. 2009, Pall Corporation.
43. Ebrahimi, A., et al., *Energetic, exergetic and economic assessment of oxygen production from two columns cryogenic air separation unit.* Energy, 2015. **90**: p. 1298-1316.
44. CREG, *A European comparison of electricity and gas prices for large industrial consumers*. 2016, PwC Enterprise Advisory.
45. DOE, *How To Calculate The True Cost of Steam*. 2003, U.S. Department of Energy

46. Okazaki, J., et al., *Importance of the support material in thin palladium composite membranes for steady hydrogen permeation at elevated temperatures.* Physical Chemistry Chemical Physics, 2009. **11**(38): p. 8632-8638.
47. Jia, H., et al., *High-temperature stability of Pd alloy membranes containing Cu and Au.* Journal of Membrane Science, 2017. **544**: p. 151-160.
48. Gallucci, F., et al., *Advances on High Temperature Pd-Based Membranes and Membrane Reactors for Hydrogen Purifcation and Production.* Journal of Membrane Science and Research, 2017. **3**(3): p. 142-156.